International Journal of Astrophysics and Space Science
2023; 11(2): 15-22
http://www.sciencepublishinggroup.com/j/ijass
doi: 10.11648/j.ijass.20231102.11
ISSN: 2376-7014 (Print); ISSN: 2376-7022 (Online)

Attitude Estimation of H2A Rocket Body from Light Curve Measurements

Alessandro Vananti[1], Yao Lu[1, 2], Thomas Schildknecht[1]

[1]Astronomical Institute, University of Bern, Bern, Switzerland

[2]Purple Mountain Observatory, Chinese Academy of Sciences, Nanjing, China

Email address:

alessandro.vananti@unibe.ch (Alessandro Vananti), yaoluastro@gmail.com (Yao Lu),
thomas.schildknecht@unibe.ch (Thomas Schildknecht)

To cite this article:

Alessandro Vananti, Yao Lu, Thomas Schildknecht. Attitude Estimation of H2A Rocket Body from Light Curve Measurements. *International Journal of Astrophysics and Space Science*. Vol. 11, No. 2, 2023, pp. 15-22. doi: 10.11648/j.ijass.20231102.11

Received: September 18, 2023; **Accepted**: October 12, 2023; **Published**: October 28, 2023

Abstract: The knowledge of the attitude motion of space debris is relevant for active debris removal missions. One possibility to characterize the attitude of space objects consists in the acquisition of photometric measurements over time, called light curves. The observed object is illuminated by the Sun and the variation of its apparent brightness gives information about its attitude state, e.g. whether the object is tumbling or not. If the light curve indicates a clear periodic variation it can be assumed that the object is rotating around its own axis with approximately constant angular velocity. However, often the orientation of the spin axis in body-fixed and inertial frame is unknown and its determination is challenging. Depending on the observed object and the information available about its shape, surface, components, a limited number of methods exists to determine the spin axis orientation. In this article we focus the attitude analysis on the Japanese H2A upper stage. Several light curves of this type of rocket body exhibit specific peaks, which can be exploited to extract attitude information. We assume that the peaks are related to the specular reflection occurring on the conical part of the upper stage. We present a novel method to estimate the direction of the rotation axis from the position of these peaks.

Keywords: Space Debris, Attitude Determination, Light Curves, H2A Rocket Body

1. Introduction

One possible solution proposed to mitigate the growing problem of space debris is Active Debris Removal (ADR). This approach has to be considered to remove large objects like e.g. upper stages or big satellites, in order to stabilize or even reduce the future debris population. Knowing the attitude state of the object candidate for removal is fundamental for the mission and for the choice of the removing procedure. Similarly, in contingency situations if the affected satellite is not responsive the knowledge of the attitude state can be helpful to understand the problem. Different observation techniques like e.g. photometric measurements, laser ranging, and radar tracking are usually employed for attitude characterization.

In photometric observations the variation of the brightness of the object as a function of time, also called light curve, provides information about the rotation of the observed object. Different studies have been performed to determine debris rotation periods from light curves [1-3]. More challenging is the determination of its attitude state, e.g. identifying the direction of a rotation axis, which may require multiple observations or techniques. In photometry, measurements can be acquired also in different spectral bands allowing a further characterization of the attitude according to surface colors of the space objects [4, 5]. A related technique is reflectance spectroscopy [6, 7], where a higher spectral resolution provides characteristic spectra of the observed surfaces that can be used as fingerprints of space components. Recently, a new method called quanta photogrammetry was successfully applied to study the attitude of the defunct Topex/Poseidon satellite [8]. Laser ranging is another technique available to study the attitude motion [9, 10]. Satellite Laser Ranging (SLR) applies to satellites equipped with retroreflectors, while newly Space Debris Laser Ranging (SDLR) considers also non-cooperative targets (without retroreflectors). The combination of more techniques can be used to refine the attitude of defunct

satellites or rocket bodies. Laser ranging was applied together with single-photon light curves e.g. in the research of Zhao et al. [11], while in the work of Silha et al. [12] beside light curves and SLR also radar measurements were performed.

Specifically to light curves, there are essentially two approaches to estimate the orientation of the space object's spin axis. Based on the formulation of Williams [13], Santoni et al. [14] determined from light curves the direction of the rotation axis of a rocket body. Their approach, called "amplitude method" bases on the ratio of the maximal and minimal brightness evaluated in the light curve and is limited to cylindrical shapes, like e.g. rocket bodies. Using another model based on the brightness ratio, Yanagisawa and Kurosaki [15] were able to compute, in addition to the spin axis, also the precession motion of a rocket body. A different way to determine the attitude relies on the so-called "epoch method" [16, 17]. In the latter the difference between apparent synodic and sidereal rotation is exploited to identify the axis of rotation.

In this work we propose a novel method to approach the attitude estimation problem for a specific class of objects with characteristics similar to the Japanese H2A upper stage. The light curves of the latter show strong specular reflection peaks coming from the conical top part of the body. In the proposed model we relate the position of these peaks to the direction of the angular velocity vector. The identified attitude is then compared with the result obtained using the amplitude method to assess the proposed model.

2. Attitude Determination Method

2.1. The H2A Rocket Body

The Japanese H2A rocket is a launch system designed to bring payloads to LEO and GTO orbits. After releasing the payload the second stage remains in orbit. This upper stage (see Figure 1) has a diameter of 4 m and a height of 9.2 m [18]. The upper part is a truncated cone with a payload adapter on the top that may differ according to the type of payload. The base of the truncated cone is 4070 mm in diameter while the upper truncated section (without adapter) has a diameter of 2190 mm. Its height without considering the adapter is 1021 mm. From these measures a cone aperture of about 47.4° is derived.

In this study we will specifically analyze the H2A rocket body (R/B) with the COSPAR designation 2010-045B. The object currently (as of 26.06.23) flies on an eccentric orbit with apogee at 9'913 km, perigee at 176 km, and inclination around 32°.

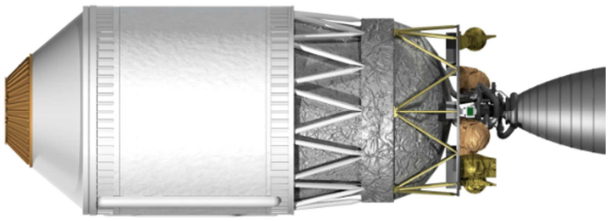

Figure 1. *H2A upper stage [19].*

2.2. Light Curves

Photometric measurements of the 2010-045B R/B are available in the database of the Mini-Mega-TORTORA (MMT) Wide Angle Surveillance System [20]. Light curves of this object were already studied by Vananti et al. [21]. In the latter the authors tried to fit the measured light curves assuming different components of the rocket body with different reflection properties. Figure 2 shows the real (in blue) and the simulated light curves with two different models (in orange and green). The authors were able to identify four characteristic sections in the light curves (see Figure 3) and associate them to components of the object. The strong characteristic "peaks" are related to the cone surface, while the adjacent "hill" section corresponds to the cylindrical part. The small peak referred as "spike" is caused by the bottom part, where the nozzle and other elements are present, while the "valley" between the peaks is attributed to the top of the object. The intervals between the strong peaks show an additional symmetry related to the rotation of the body w.r.t. the Sun and the observer. In the following a method is proposed to determine the rotational axis of the body from the position of these peaks.

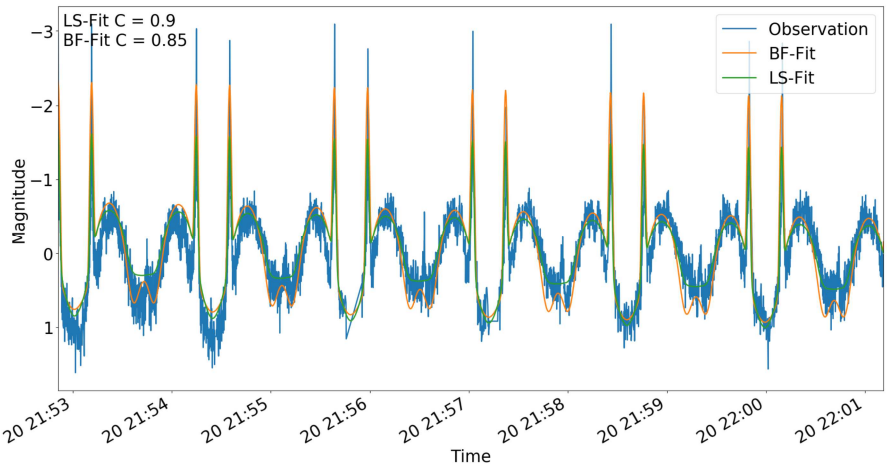

Figure 2. *Real and simulated light curves of H2A rocket body 2010-045B observed on 2018-09-22 [21].*

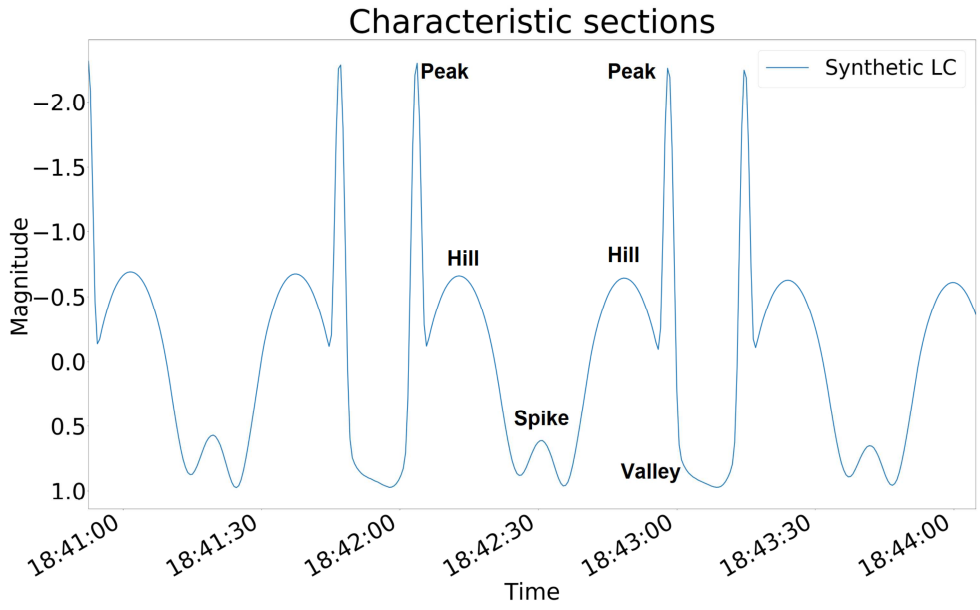

Figure 3. *Characteristic sections of the light curve [21].*

2.3. Spin Axis Determination

The method assumes that the object is in flat spin state with a constant rotation axis h and constant angular momentum H. The latter are perpendicular to the axis of symmetry, in the following denoted as s, of the cylindrical R/B and of the cone on the top. Figure 4 shows a schematic picture of the problem.

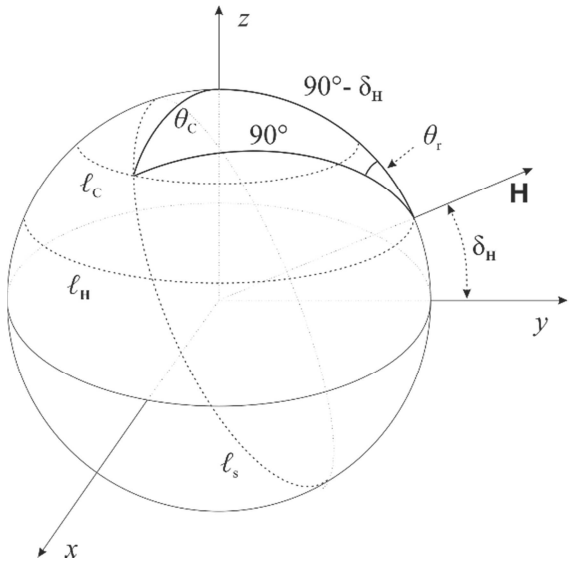

Figure 4. *Scheme showing the angular momentum direction H w.r.t. the phase angle bisector in z direction. The condition for specular reflection is given at the intersection of ℓ_s (possible orientations of the body) and ℓ_C (possible cone orientations for specular reflection).*

We consider a system of coordinates x, y, z where z is parallel to the phase angle bisector and H lies in the y-z plane. In this system, directions correspond to lines passing through the center of the sphere and are represented by their intersection points (projection) on the unit sphere. The direction of the angular momentum H can be described in spherical coordinates with elevation angle δ_{H} and azimuthal angle $\alpha_{\mathrm{H}} = 90°$. We know that specular reflection occurs when the bisector is perpendicular to a surface of the object. The latitude line ℓ_{C} shows the possible directions of the axis s of the cone that satisfy specular reflection, i.e. with a plane tangent to the cone and perpendicular to the bisector z. The zenith angle at this latitude is equal to the cone aperture angle θ_{C}. On the other hand, the line ℓ_{s} shows the directions covered by s during the rotation of the body around the axis h parallel to H. In fact, ℓ_{s} lies in a plane perpendicular to H and, since the object is in flat spin, ℓ_{s} is a great circle on the sphere. The intersection of ℓ_{C} and ℓ_{s} is the orientation of s which satisfies the specular reflection condition. From this intersection point a spherical triangle with the sides θ_{C}, 90°, and $90°-\delta_{\mathrm{H}}$ can be constructed. The angle θ_{r} in the triangle is measured on the great circle ℓ_{s} between the intersection point and the y-z plane. An equivalent specular reflection condition can be found at an angle $-\theta_r$ in the opposite position w.r.t. that plane.

Referring to Figure 3 we can define the time interval between two close peaks with t_p and we can determine the period T of the light curve. According to the presented model, the two peaks are identified with the orientations at $-\theta_r$ and θ_r in which specular reflection occurs. Note from the construction in Figure 4 that $\theta_{\mathrm{r}} \leq \theta_{\mathrm{C}}$ always applies and since $\theta_{\mathrm{C}} < 90°$ the interval t_p is always the time between the two closest peaks, i.e. less than half of the period.

We define the angular velocity ω of the body parallel to H and we describe its orientation with the angle θ_r along the great circle ℓ_{s}. Then, from $|\omega|T = 2\pi$ and $|\omega|t_p = 2\theta_r$ we have:

$$\theta_r = \frac{\pi\, t_p}{T}. \tag{1}$$

Thus, θ_r can be obtained from the measured light curve and, if the aperture angle of the cone θ_{C} is known, the angle

δ_H can be calculated applying the spherical law of cosines to our case as $\cos\theta_C = \cos\theta_r \cos\delta_H$. It follows:

$$\delta_H = \pm\text{acos}\left(\frac{\cos\theta_C}{\cos\theta_r}\right). \quad (2)$$

Eq. (2) shows two possible solutions with different sign and these exist only for $\theta_r \leq \theta_C$. It is easy to see in Figure 4 that the case with an angular momentum vector H at $-|\delta_H|$ equally satisfies the specular reflection condition. It is also clear from our construction that for any direction of H along the latitude ℓ_H, i.e. with same δ_H, the same reflection conditions apply, being the zenith angle w.r.t. the bisector z constant. The solution set with $-|\delta_H|$ is equivalent to the one with $+|\delta_H|$ up to the sense of rotation of the body (+H or −H), which cannot be determined with this approach. Thus, in the following we will consider only the solution with $+|\delta_H|$. From the above construction it becomes evident that from one light curve of the object it is not possible to determine a unique spin axis orientation.

To further constrain the problem another light curve is necessary, providing a new δ'_H value w.r.t. another bisector z'. The intersection of the two circles ℓ_H and ℓ'_H gives two common solutions for the rotation axis. Figure 5 illustrates the idea to identify the intersection points. The vectors c and c′ indicate the centers of the circles ℓ_H and ℓ'_H, respectively. We want to find the length ℓ in the triangle *EFG* and we see that the angle α is equal to the one between c and c′. The side d is calculated as $d = \frac{|c'|}{\cos\alpha} - |c|$ and we can determine ℓ using $\ell = \frac{d}{\tan\alpha}$. The radius r_H of the circle ℓ_H is given by $r_H = \cos\delta_H$. The distance p between G and the intersection points P_1 and P_2 is $p = \sqrt{r_H^2 - \ell^2}$. Thus, in the shown reference system, with the bisector z and the y-z plane containing z and z', the points P_1 and P_2 are defined through the components $\pm p$, ℓ, $|c|$. Note that the sign of ℓ depends on whether the angle α from c to c′ is clockwise or not, and whether $|c| < |c'|$ or not, and needs to be determined accordingly. Once the coordinates of the intersections are found they need to be transformed with a rotation matrix into the inertial system.

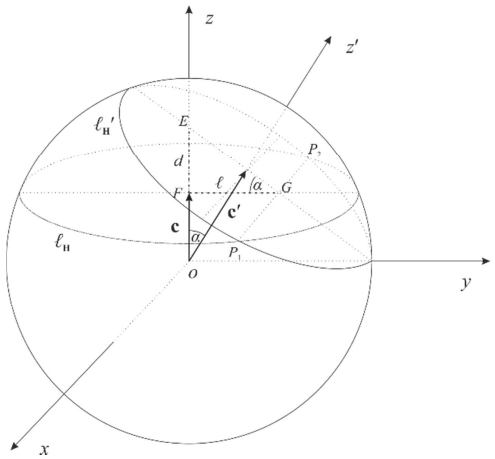

Figure 5. *Scheme showing the intersection P_1 and P_2 of the two circles ℓ_H and ℓ'_H related to the bisector z and z', respectively.*

As we have seen, owing to the information coming from two light curves we are able to constrain the problem to two possible solutions P_1 and P_2. The same procedure can be applied using a third measurement with another bisector z'' and obtaining two new solutions Q_1 and Q_2. If z, z', and z'' are not coplanar there is a unique combination i, j with $P_i = Q_j$ and thus a unique solution for the rotation axis. The solution is a vector on the unit sphere and can be represented in the inertial system with coordinates in right ascension and declination. Note that the sense of rotation is not defined and the solution is equivalent to the opposite vector.

3. Attitude Estimation from Real Measurements

3.1. Method Using Peak Distance

We considered the light curves of the H2A R/B (2010-045B) from the MMT catalogue for the four consecutive nights from 19.09.2020 to 22.09.2020 (Figure 6 to Figure 9).

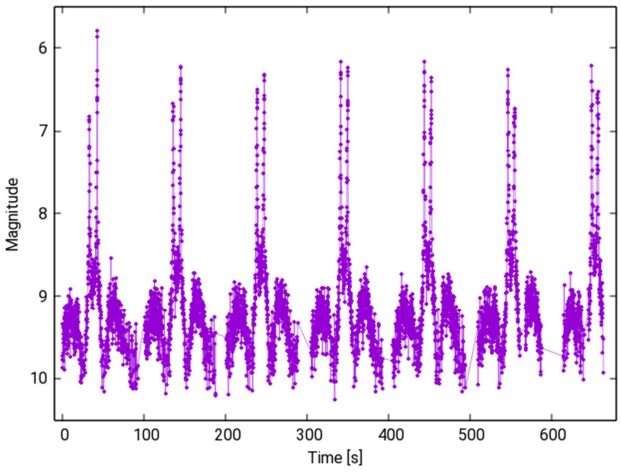

Figure 6. *Light curve of H2A R/B (2010-045B) taken from MMT catalogue. Time elapsed since 19.09.2020, 22:04:46.*

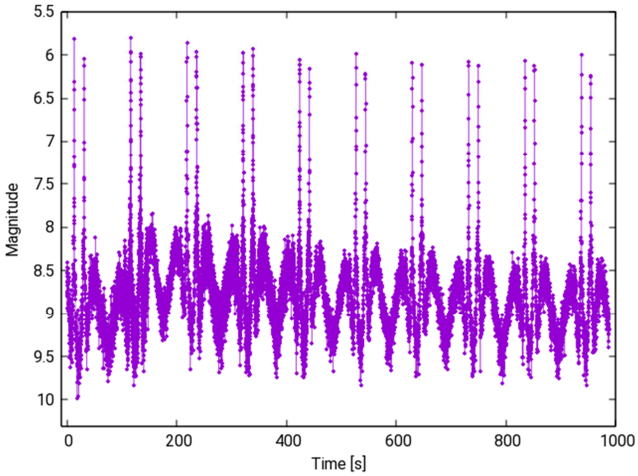

Figure 7. *Light curve of H2A R/B (2010-045B) taken from MMT catalogue. Time elapsed since 20.09.2020, 21:05:32.*

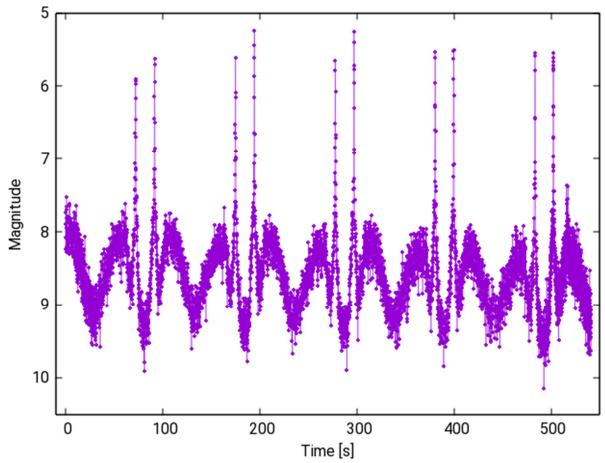

Figure 8. *Light curve of H2A R/B (2010-045B) taken from MMT catalogue. Time elapsed since 21.09.2020, 21:26:29.*

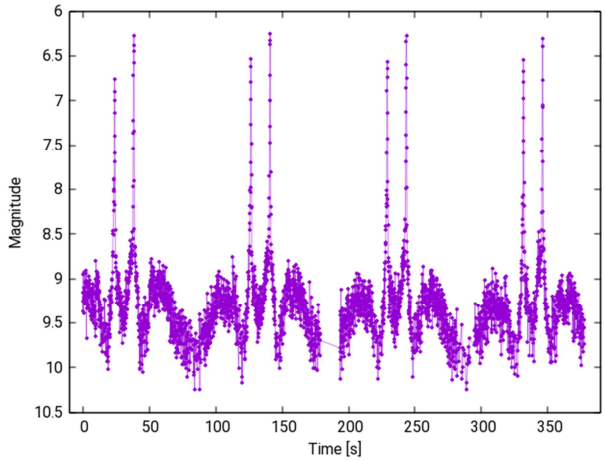

Figure 9. *Light curve of H2A R/B (2010-045B) taken from MMT catalogue. Time elapsed since 22.09.2020, 23:56:18.*

The position of the peaks were determined with the Matlab script *findpeaksSG.m* [22], where a Gaussian fit of the peaks is performed. Table 1 indicates measured time intervals, ratio t_p/T, δ_H, and average bisector for every measurement. The standard deviation of the measured intervals is indicated, as well as the numerical propagated uncertainty in δ_H. The bisector is calculated using TLE orbits of the given date downloaded from SpaceTrack catalogue on www.space-track.org. The TLE orbits are propagated with a SGP4 model to the mid epoch of the light curve and from the position of object and Sun, the bisector direction is determined. For the latter computation the *Skyfield* python module was used [23]. The uncertainty in the bisector is given by the change of the object position during the measured passage. Using the mid epoch provides an approximate average position. We see that the uncertainty reaches some degrees and is higher than the one in δ_H. Looking at our geometric approach, it is expected to have the largest impact on the accuracy of the solution.

According to the procedure in the previous section, from two given ratios t_p/T two possible solutions are obtained. Since we have more than two light curves available we consider solutions computed with pairwise combinations of them. Figure 10 illustrates the obtained solutions from possible combinations of the four measurements. The two solutions of every combination are indicated with same symbol and color. Since we expect a unique solution we discard the dispersed points in the region above 300° right ascension and 55° declination and we focus on the other ones in the bottom left of the figure which seem to provide a common solution (see detail in Figure 11). The points are confined in a relatively small range of 5° in right ascension and 2° in declination.

Table 1. *Time intervals, ratio t_p/T, δ_H, and average bisector for all light curves.*

No.	Date	t_p [s]	T [s]	t_p/T	δ_H [°]	z (ra [°])	z (dec [°])
1	19.09.2020	8.7 ± 0.7	102.80 ± 0.04	0.085 ± 0.007	40.7 ± 0.4	206.1 ± 1.3	-14.030 ± 0.002
2	20.09.2020	17.5 ± 0.3	102.62 ± 0.04	0.171 ± 0.003	33.3 ± 0.5	177.6 ± 2.7	-7.2 ± 1.5
3	21.09.2020	19.3 ± 0.3	102.82 ± 0.03	0.187 ± 0.003	28.4 ± 0.4	163.4 ± 2.7	0.4 ± 2.0
4	22.09.2020	14.3 ± 0.03	102.57 ± 0.01	0.1401 ± 0.0003	36.05 ± 0.04	194.4 ± 1.5	-14.1 ± 0.3

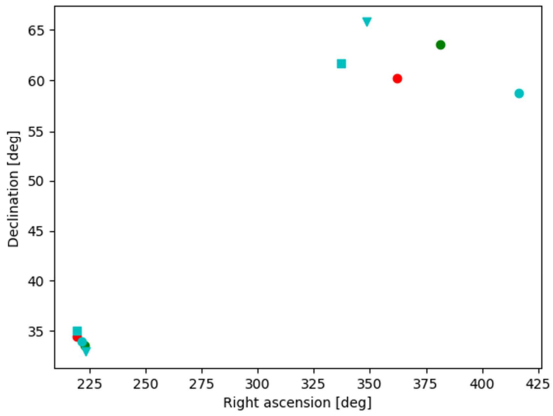

Figure 10. *Spin axis solutions obtained with pairwise combination. Every combination has two solutions indicated with same symbol and color.*

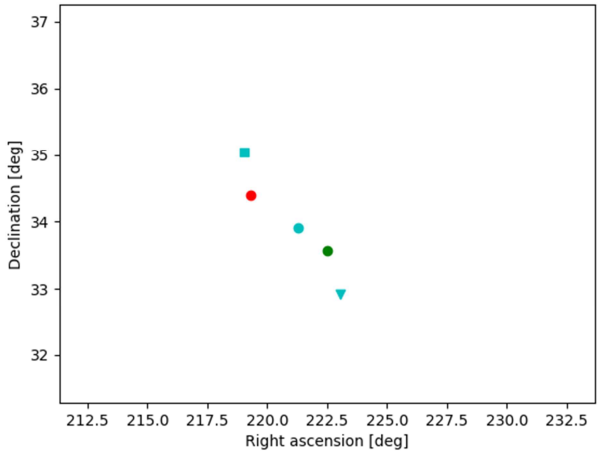

Figure 11. *Bottom left detail of Figure 10.*

In Table 2 the confined solutions in right ascension and declination for the combinations are given. The first column indicates which measurements are combined and the indices refer to the first column in Table 1. The standard deviation in right ascension and declination of the obtained axis h, as well as the covariance are listed. The latter were computed propagating numerically the uncertainty in δ_H and in the bisector z through the procedure illustrated in Figure 5. The range covered by σ_{ra} and σ_{dec} is in the same order of magnitude as the dispersion of the solutions. For the final determination of the spin axis of the object we consider the average solution over all the combinations, which is shown in the last row of Table 2.

In general, the computed standard deviation, although in the same order of magnitude, seems to be smaller than the dispersion of the solution values. This indicates that in the model used for the uncertainty we do not consider all possible sources of errors. In our model we assume e.g. that the spin axis of the object remains constant during the period covered by the observations. However, this cannot be always guaranteed. In the case of the H2A R/B (2010-045B) the orbit has a perigee below 200 km and drag forces are among the dominant perturbations in addition to eddy currents and gravity gradient forces. A precession of the spin axis may occur under the influence of these forces and the change of the orientation can be of several degrees within few days for R/B in LEO orbits [24].

Table 2. *Results for all combinations and average solution. Indices in first column refer to measurement number in Table 1. Direction of rotation axis h, related standard deviation in right ascension, declination, and covariance are indicated.*

Comb.	h (ra [°])	h (dec [°])	σ_{ra} [°]	σ_{dec} [°]	$\sigma_{\mathrm{ra,dec}}$ [deg^2]
1, 2	222.5	33.5	2.0	1.0	-1.6
1, 3	219.3	34.4	1.4	0.7	-0.6
1, 4	221.3	33.9	3.2	1.4	-4.1
2, 4	223.1	32.9	2.9	2.0	-5.6
3, 4	219.0	35.0	1.6	1.0	-1.5
Avg.	221.0	33.9	2.4	1.6	-3.3

3.2. Comparison with Amplitude Method

We can compare the obtained results with the so-called "amplitude method" [14]. The idea of the method bases on the difference of magnitude between periodic maxima and minima (i.e. amplitude) in the light curve due to the rotation of the body and to diffuse reflection on its surface. This amplitude depends on the position of the object w.r.t. Sun and observer, and on the orientation of the spin axis. The method works for cylindrical objects (like e.g. rocket bodies) assuming no reflection from their top or bottom part and assuming a constant spin axis.

For the processing of the data we follow the steps also referred in the work of Vananti et al. [25]. The light curves of the four nights were linear detrended, smoothed with cubic splines, and the maximal and minimal value were found within every period and averaged. Note that, referring to Figure 3, to be consistent with the cylindrical model we have to detect the maximum in the "Hill" and the minimum in the "Valley" section, and not the absolute maximum reached in the peaks. In the light curves in Figure 6 and Figure 9 the "Valley" does not reach the minimum and the small minima beside the "Spike" are selected instead. Table 3 shows the phase angle, the average amplitude and its standard deviation extracted from the measurements. To calculate the phase angle, the orbit was propagated as in the previous method and the mid epoch of the light curve was chosen. From the identified amplitudes a set of possible solutions for the spin axis in right ascension and declination for each of the four observations is computed. Figure 12 displays the sets of solutions with four different colors. From the figure it is not so well visible, but zooming in the single possible intersection regions reveals that the four solution sets overlap only in the region with right ascension between -150° and -100°. The overlapping region is detected with a software procedure and is illustrated in Figure 13 as green area in the detailed portion of the diagram. The mean value of the intersecting area is -139.5° in right ascension (equivalent to a positive value of 220.5°) and 30.4° in declination with standard deviations σ_{ra} = 2.3°, σ_{dec} = 2.9° and covariance $\sigma_{\mathrm{ra,dec}}$ = -5.7 deg^2. The computed values are comparable with the values 221° and 33.9° found in the previous method using the peak distance and they roughly lie within the predicted uncertainty. This result brings further evidence in the validity and consistency of the above proposed approach.

Table 3. *Phase angles, amplitudes and standard deviations for the four light curves.*

Epoch	Phase angle [deg]	Amplitude	Std. deviation
19-Sep-2020 22:10:00	67	-1.2	0.2
20-Sep-2020 21:13:00	16	-1.4	0.1
21-Sep-2020 21:31:00	31	-1.7	0.3
23-Sep-2020 00:02:00	40	-1.1	0.2

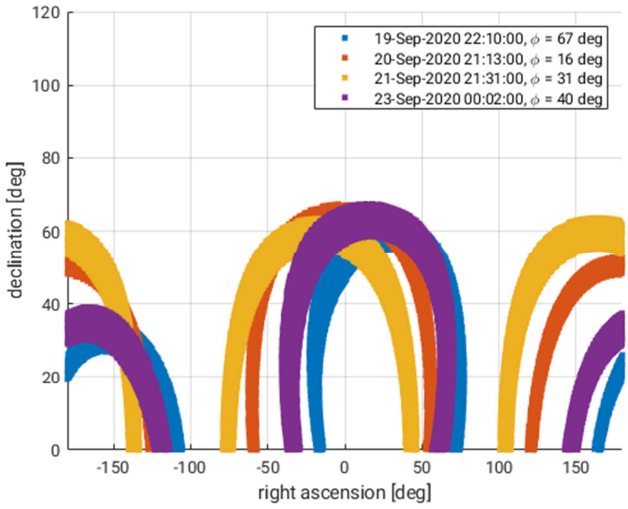

Figure 12. *Solution sets computed for the four light curves.*

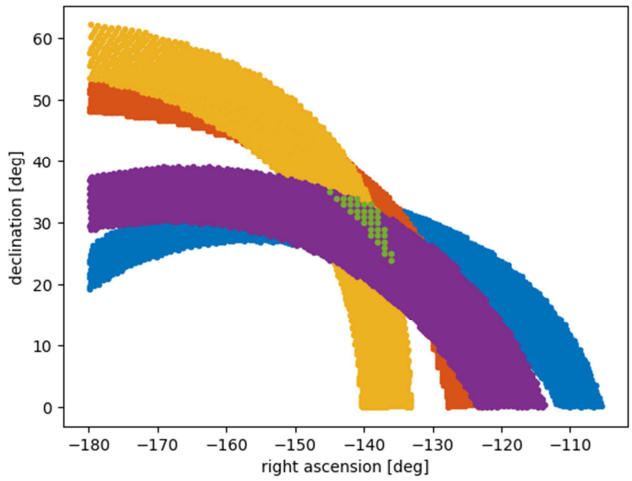

Figure 13. *Detail of the diagram in Figure 12 showing the intersection region in green.*

4. Conclusions

A novel method to determine the spin axis orientation of space objects with a conical surface was developed. The approach bases on different light curve measurements of the object and assumes that its spin axis remains constant during the overall interval covering the observations. Specular reflection at the conical surface produces peaks in the light curves and according to their relative position it is possible to determine the orientation of the spin axis. The method necessitates at least three light curves to find a unique solution for the orientation. In the procedure the combination of two measurements provides two possible solutions. Another combination with a third measurement will have one solution in common with the first combination and the latter is the searched unique solution.

The approach was tested on four observations on consecutive nights of an H2A rocket body (2010-045B) taken from the MMT catalogue. The pairwise combination of the acquired light curves provides a delimited common region in right ascension and declination attributed to the orientation of the rotation axis. The dispersion of the single solutions allows the characterization of the statistical uncertainty. The latter is mainly caused by the slightly change of the bisector direction during the observation passage of the object, while in the procedure an average constant bisector is assumed. For the reported case an error of few degrees in the orientation was identified. Additional uncertainty in the solution can be related to the assumption of a constant rotation axis during the interval of observations. In fact, space objects are subject to different types of forces in orbit that can considerably change the spin axis direction and increase the level of uncertainty.

The obtained results were compared with the axis determined using the amplitude method, which can be applied to cylindrical shapes and thus to the non-conical part of the H2A R/B. According to this method, the maxima and minima extracted from the four light curves provide different sets of possible solutions and the common intersection defines the orientation of the spin axis. The solutions found with both approaches are consistent within few degrees in agreement with the computed uncertainty. This further result confirms the validity of the proposed method.

In this paper, the procedure was applied to a specific space object and to observations that contain bright peaks due to specular reflection on its conical component. In general, depending on the attitude of the object the condition for reflection will not be always satisfied and depending on the surface the peaks will more or less pronounced. In those cases where this procedure is applicable, it provides a valid alternative to other approaches like e.g. the amplitude method, especially where only a conical and not a cylindrical shape is present or the reflectivity of the top and bottom part of the cylindrical body is not negligible. We have seen that the assumption of a constant bisector averaged over the light curve duration introduces uncertainties in the axis determination. On the other hand, considering the peak distance only at a single epoch within the light curve would not take advantage of the statistical distribution of the distances. In this regard, further investigations are envisaged in the future in order to improve the current algorithm and the accuracy of the axis determination.

References

[1] Earl MA, Wade GA (2014) Observations and analysis of the apparent spin period variations of inactive boxwing geosynchronous resident space objects. In: Proceedings of 65th International Astronautical Congress, Toronto, Canada.

[2] Silha J, Pittet JN, Hamara M, Schildknecht T (2018) Apparent rotation properties of space debris extracted from photometric measurements. Advances in Space Research 61: 844-861.

[3] Silha J, Krajcovic S, Zigo M, Toth J, Zilkova D, Zigo P, Kornos L, Simon J, Schildknecht T, Cordelli E, Vananti A, Mann HK, Rachman A, Paccolat C, Flohrer T (2020) Space debris observations with the Slovak AGO70 telescope: Astrometry and light curves. Advances in Space Research 65: 2018-2035.

[4] Cardona T, Seitzer P, Rossi A, Piergentili F, Santoni F (2016) Bvri photometric observations and light-curve analysis of geo objects. Advances in Space Research 58: 514-527.

[5] Lu Y, Zhang C, Sun R, Zhao C, Xiong J (2017) Investigations of associated multi-band observations for geo space debris. Advances in Space Research 59: 2501-2511.

[6] Vananti A, Schildknecht T, Krag H (2017) Reflectance spectroscopy characterization of space debris. Advances in Space Research 59: 2488-2500.

[7] Zilkova D, Silha J, Matlovic P, Toth J (2023) Space debris spectroscopy: Specular reflections at LEO regime. Advances in Space Research 71: 3249–3261.

[8] Kucharski D, Kirchner G, Jah M, Bennett JC, Koidl F, Steindorfer M, Wang P (2021) Full attitude state reconstruction of tumbling space debris TOPEX/Poseidon via light-curve inversion with Quanta Photogrammetry. Acta Astronautica 187: 115-122.

[9] Kucharski D, Kirchner G, Koidl F, Fan C, Carman R, Moore C, Dmytrotsa A, Ploner M, Bianco G, Medvedskij M (2014) Attitude and spin period of space debris Envisat measured by Satellite Laser Ranging. IEEE Transactions on Geoscience and Remote Sensing 52: 7651-7657.

[10] Pittet JN, Silha J, Schildknecht T (2018) Spin motion determination of the Envisat satellite through laser ranging measurements from a single pass measured by a single station. Advances in Space Research 61: 1121-1131.

[11] Zhao S, Steindorfer M, Kirchner G, Zheng Y, Koidl F, Wang P, Shang W, Zhang J, Li T (2020) Attitude analysis of space debris using SLR and light curve data measured with single-photon detector. Advances in Space Research 65: 1518-1527.

[12] Silha J, Schildknecht T, Pittet JN, Kirchner G, Steindorfer M, Kucharski D, Cerutti-Maori D, Rosebrock J, Sommer S, Leushacke L, Kärräng P, Kanzler R, Krag H (2017) Debris attitude motion measurements and modelling by combining different observation techniques. Journal of the British Interplanetary Society 70: 52-62.

[13] Williams V (1979) Location of the rotation axis of a tumbling cylindrical earth satellite by using visual observations: Part I: Theory. Planetary and Space Science 27: 891-894.

[14] Santoni F, Cordelli E, Piergentili F (2013) Determination of disposed-upper-stage attitude motion by ground-based optical observations. Journal of Spacecraft and Rockets 50: 701-708.

[15] Yanagisawa T, Kurosaki H (2012) Shape and motion estimate of LEO debris using light curves. Advances in Space Research 50: 136-145.

[16] Hall D, Africano J, Archambeault D, Birge B, Witte D, Kervin P (2006) AMOS observations of NASA's IMAGE satellite. In: Proceedings of AMOS Advanced Maui Optical and Space Surveillance Technologies Conference, Maui, Hawaii, US.

[17] Hall D, Kervin P (2014) Optical characterization of deep-space object rotation states. In: Proceedings of AMOS Advanced Maui Optical and Space Surveillance Technologies Conference, Maui, Hawaii, US.

[18] Mitsubishi Heavy Industries Ltd (2015) H-IIA User's Manual. https://www.mhi.com/jp/products/pdf/manual.pdf. Accessed 15 June 2023.

[19] Japan Aerospace Exploration Agency (2015) About H-IIA Launch Vehicle. https://global.jaxa.jp/projects/rockets/h2a/index.html. Accessed 15 June 2023.

[20] Karpov S, Katkiva E, Beskin G, Biryukov A, Bondar S, Davydov E, Ivanov E, Perkov A, Sasyuk V (2016) Massive photometry of low-altitude artificial satellites on Mini-Mega-TORTORA. Revista Mexicana de Astronomia y Astrofisica 48: 112-113.

[21] Vananti A, Guthruf D, Lu Y, Schildknecht T (2021) Estimation of reflective properties from light curves of H2A rocket body. In: Proceedings of 8th European Conference on Space Debris, Darmstadt, Germany.

[22] O'Haver T (2016) Segmented peak finder findpeaksSG.m. MATLAB Central File Exchange. https://www.mathworks.com/matlabcentral/fileexchange/60301-segmented-peak-finder-findpeakssg-m. Accessed 15 June 2023.

[23] Rhodes B (2019) Skyfield: High precision research-grade positions for planets and Earth satellites generator. Astrophysics Source Code Library ascl: 1907.024. http://rhodesmill.org/skyfield/. Accessed 15 June 2023.

[24] Ojakangas G, Anz-Meador P, Cowardin H (2012) Probable rotation states of rocket bodies in Low Earth Orbit, In: Proceedings of AMOS Advanced Maui Optical and Space Surveillance Technologies Conference, Maui, Hawaii, US.

[25] Vananti A, Kucharski D, Steindorfer MA, Kanzler R, Kärräng P, Cerutti-Maori D, Rosebrock J, Schildknecht T (2023) Multi-sensor space object tracking for tumbling motion characterization. In: Proceedings of 2nd ESA NEO and debris detection conference, Darmstadt, Germany.